Single Pt atom stabilized on nitrogen doped graphene: CO oxidation readily via the tri-molecular Eley-Rideal mechanism

Xilin Zhang[a], Zhansheng Lu[*a], Guoliang Xu[a], Tianxing Wang[a], Dongwei Ma[b], Zongxian Yang[*a], and Lin Yang[c]

Single-atom catalysts, especially for the single Pt atom, have attracted more and more attentions due to their high catalytic activity to CO oxidation. The outstanding stability and catalytic activity of single Pt atom supported on nitrogen doped graphene (Pt/NG) are revealed using the first-principles calculations. We find that the stability of Pt atom on NG can be promoted by picking up appropriate doping configuration. The exceptionally stable Pt/NG catalyst exhibits excellent catalytic activity to CO oxidation via a new tri-molecular Eley-Rideal mechanism ($2CO + O_2 \rightarrow OCO\text{-}OCO \rightarrow 2CO_2$) with an energy barrier of 0.16 eV for the rate-limiting step of OCO-OCO dissociation, which is more preferable than the other two normal Langmuir-Hinshelwood and Eley-Rideal mechanisms.

1. Introduction

The oxidation of CO has attracted great interest because it is of great importance to solve the growing environmental problems caused by CO emission. The earlier studies found that some noble metals can effectively catalyze CO oxidation.[1-4] However, they are costly and require high reaction temperatures for efficient operations. Considerable efforts have been made to develop novel and efficient catalysts for low temperature CO oxidation.[5-8]

Downsizing the size of particles is an important way to lower the consumption of catalysts while keep the catalytic performance. Based on this principle, the isolated[9] or supported[10] single atom catalysts have drawn more research attention since the unsaturated coordination metal atom can act as activated site for gas adsorption. Indeed, some studies proved that the single metal atom catalyst exhibits superior catalytic activity to CO oxidation[11-14] as compared with conventional metal catalysts. Zhang et al.[15] found that the Pt single-atom catalyst, which was synthesized by assembling Pt single-atom into the surface defects of iron oxide nanoparticles, exhibits prominent activity and stability for CO oxidation. As the size of metal nanoparticles goes down to single-atom, the interaction of the single metal atom with substrate is apparent important to the stability and catalytic performance of the complex catalyst. Besides, the supported catalysts are usually desired to disperse finely on a substrate with a high surface area for using the active components efficiently. Recently, the chemically modified graphene has been suggested as an effective method to solve the problem of weak interaction between the metal atom and the pristine graphene substrate[16] while keep the advantage of huge surface-to-volume ratio for graphene. Additionally, the modified graphene could also be regarded as gas sensor[17] or direct catalyst.

One important method to modify graphene is chemically doping with other atoms to tune the local curvature and electronic redistribution, and of course the chemical properties of the graphene. For example, the N[18-20] and P[21-23] doped graphene systems were synthesized by different methods and confirmed with an enhanced catalytic activity for oxygen reduction reaction both in recent experimental studies[23,24] and theoretical calculations.[25,26] Our previous first-principles calculations found that the N doped graphene (NG) is an efficient catalyst for NO reduction.[27,28] Wang et al. reported that the NG could be used as the biosensor for glucose.[29] Interestingly, the recent experiment studies indicated that the NG could be used not only as the direct catalyst but also as a good substrate to stabilize the Pt nanoparticles catalyst.[30,31] Xiong's group also pointed out that the improved dispersion, uniformity and smaller size of the Pt metal particles by N-doping were beneficial to catalytic activity towards the methanol oxidation.[30] Some theoretical works also proved that the stability of single atom Pt supported on graphene can be improved by some nonmetal[12,32,33] or metal[34] dopants as compared with that on undoped graphene[16], and the catalytic activity for CO oxidation can also be promoted.

Motivated by above mentioned experimental and theoretical results, the stability and catalytic activity of single atom Pt supported on NG are explored. The entire reaction process of CO oxidation on the selected most stable Pt/NG is investigated. It is found that the tri-molecular E-R mechanism[7] is more preferable than the other two mechanisms from energy barrier respect.

2. Computational method

The spin-unrestricted density functional theory (DFT) calculations are performed by the DMol3 code[35] embedded in Materials Studio. A double numerical plus polarization (DNP) is used as the basis setup, while the ion–electron interaction is described by DFT semicore pseudopotentials (DSPPs). In order to describe the van-der-Waals (vdW) interactions between the reactants or the intermediates and the substrate, empirical dispersion-corrected density functional theory (DFT-D)[36] is used in all calculations. The exchange and correlation functional of Perdew, Burke and Ernzerhof (PBE)[37] within the generalized gradient approximation (GGA) is used for structure relaxation and energy minima. The convergence criteria are set to 10^{-5} Ha for the energy, 0.002 Ha/ Å for the force, and 0.005 Å for the displacement. The smearing value of 0.005 Ha is set to achieve self-consistent field convergence. The vacuum layer is set to 15 Å to avoid the interactions among mirror images. The linear synchronous transition/quadratic synchronous transit (LST/QST) tools[38] are used to identify the minimum energy pathway (MEP), which have been well validated to locate the transition state (TS) structure and the MEP. The reciprocal space is sampled with (5x5x1) k-points grid generated automatically using the Monkhorst–Pack method for the relaxation calculation and TS search. Moreover, the frequency analysis was carried out to confirm whether there is no imaginary frequency for every stable structures and only one imaginary frequency for each TS.

The adsorption energy is defined by the formula: $E_{ads} = E_{Sub} + E_X - E(_{X/Sub})$, where $E(_{X/Sub})$ and E_{Sub} are the total energies for the optimized equilibrium configurations of the substrate with and without gas adsorbate (X), respectively, and E_X is the total energy of the corresponding isolated molecule in its ground state. With this definition, a higher E_{ads} value means a stronger adsorption.

3. Results and discussions

3.1. Models Analysis

Generally, stability is a prerequisite of catalyst in practice. Although the adsorption ability of graphene to the single-atom Pt could be improved by doping sole N atom, the diffusion and agglomeration of Pt are inevitable due to the small diffusion barrier. More and centralized active sites need be created to enhance the adsorption and inhibit the diffusion of Pt effectively. Our previous studies proved that the graphene with three C atoms replaced by N atoms (Tri-NG) possesses centralized active sites to catalyze NO reduction[27,28]. Some earlier studies pointed out that the quaternary N doping also accounts for the high ORR activity of NG and their population can be controlled by the fabrication method [39]. Recently, the N_4-macrocyclic structure has been prepared successfully[40-42] and the foreign metal atoms coupled with this kind of N_4 structure forming the metal-N_4 system were also widely recognized as an efficient oxygen reduction catalysts[43-46]. Moreover, our previous works proved that the C-dimer surrounded by the N dopant atoms is the real activated site for reactants adsorption and reaction[27,28,47]. Combining the experimental and computational results, we further replace the central metal atom surrounded by four N atoms with two nonmetallic C atoms to restructure the activated C-dimer site for stabilizing the adsorbed Pt atom, which is not exactly the same with the experimental model. Besides, the same doping configuration has also been proved with a high performance for oxygen reduction by Feng et al[48]. So we select the configuration with four C atoms replaced by N atoms as the substrate of Pt single atom catalyst, as shown in Fig. 2a, due not only to its low cost and high-efficiency for some reactions, but also to its excellent capacity for stabilizing Pt atom. It is found that the Pt atom tends to adsorb at the bridge site of C-dimer (Fig. 2b) with an adsorption energy of 3.41 eV, which is quite larger than that on pristine[16] and other heteroatom doped graphene[12,14,32]. The slightly elongated N-C and C-C bonds caused by Pt adsorption forcing the activated central C atoms protruding from the NG plane by about 0.05 Å and the surrounding N atoms moving slightly out of the basal plane accordingly. The Mulliken charge analysis[49] indicates that the Pt atom which captures about 0.26 e from the NG sheet (mainly from the C-dimer) will serve as the active center of reactions, as shown in Table 1. The large number of charge transfer as well the quite large adsorption energy are beneficial to stabilize the Pt atom. Actually, all possible stable adsorption sites of Pt are summarized in Fig. 1 for exploring the pathway of Pt diffusion conveniently. The most possible diffusion pathway of Pt on Tet-NG is from site 1 to site 2, as shown in Fig. 2, which has a barrier of 1.65 eV. The diffusion of Pt from site 1 to site 3 has a barrier of 1.88 eV, which is about 0.23 eV larger than that from site 1 to site 2. The large barrier maybe caused by the devious diffusion pathway from site 1 to site 3 and also the Pt atom at site 3 is energetically less stable than those on sites 1 and 2 (higher in energy by about 1.04 and 0.44 eV, respectively). The similar phenomenon was observed in the process of Pt migration from site 1 to site 4. The diffusion barrier of Pt on Tet-NG (1.65 eV) is also higher than that on pristine (0.19 eV)[16], Tri-NG

(1.39 eV) and even is close to that on metal Ge doped graphene (1.62 eV)[34]. These results indicate that the Tet-NG substrate could efficiently stabilize the adsorbed single Pt atom and inhibit its diffusion and agglomeration. We further define the average binding energy: $E_{binding} = \{E(Sub) + nE(Pt) - E(Pt_n/Sub)\}/n$ to evaluate the tendency of Pt dimer formation, which has been adopted to investigate the clustering properties of the Rh atoms on CeO_2[50]. In this equation, E(Sub), E(Pt), and $E(Pt_n/Sub)$ are the total energies of the Tet-NG substrate, a free Pt atom, and the fully relaxed Pt_n/Sub system, respectively. The average binding energy of single Pt on Tet-NG (3.41 eV) is slightly larger than that of Pt dimer (3.03 eV). This result indicates that the Pt-support interaction is stronger than the Pt-Pt interaction and the Pt atoms tend to dispersedly adsorb on Tet-NG rather than forming cluster. Although there have been no experimental report on the graphene based single atom catalyst, the single atom supported on the metal oxide substrates have been realized successfully[51-55]. There have been also many theoretical works of the single metal atom supported on modified graphene with various doping patterns reported[14,33,34]. So in present paper we focus on studying the stability and activity of single Pt atom on the metal-free modified Tet-NG support. The growth mechanism of Pt clusters on Tet-NG and the catalytic activity of the complex catalysts will be studied in the future.

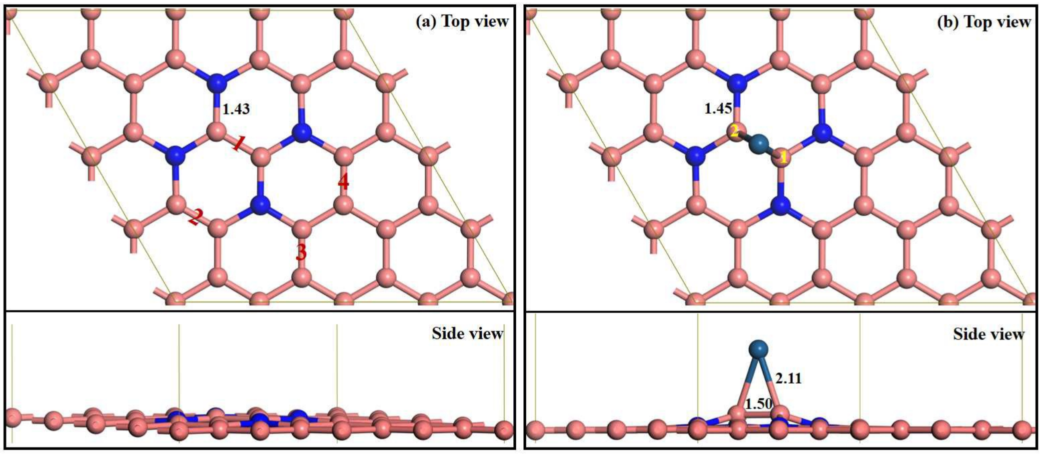

Fig. 1 The model of nitrogen doped graphene model without (a) and with (b) supported Pt. The symbols 1, 2, 3, and 4 are the most, second, third, and fourth stable adsorption site of Pt. Hereafter, the pink, blue and bice spheres are C, N and Pt atoms.

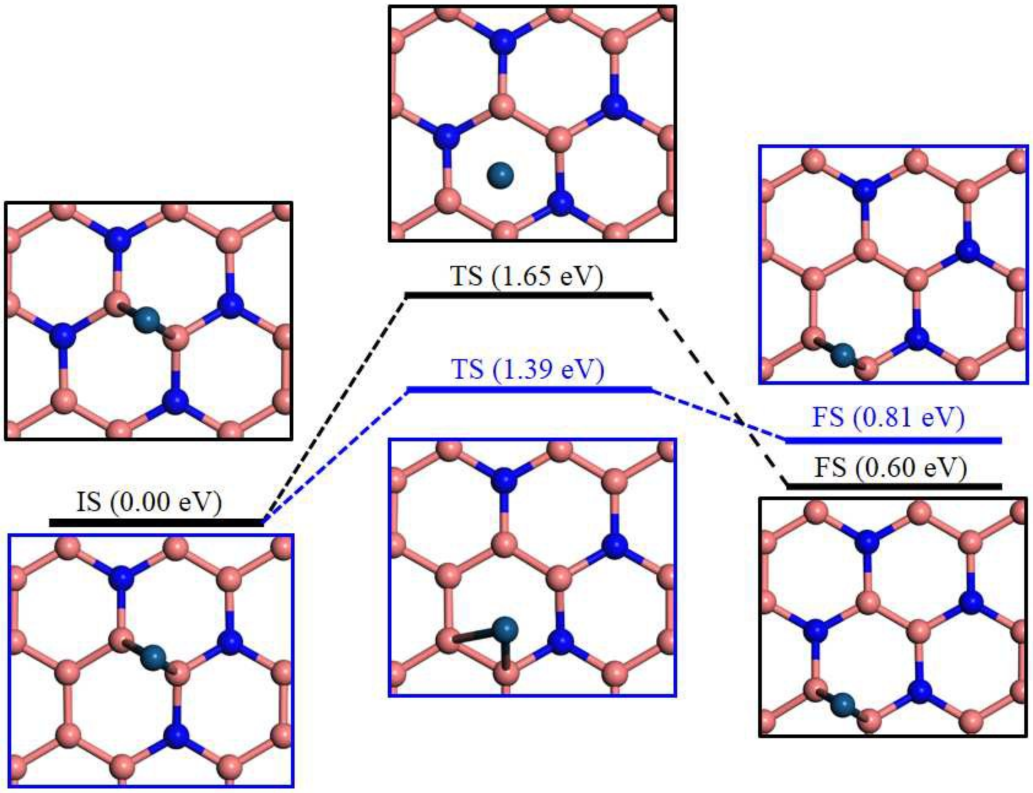

Fig. 2 The most possible diffusion of Pt on Tri-NG (blue line) and Tet-NG (black line).

Table 1. The Mulliken charges of the preferable adsorption configurations (Conf.). The positive and negative numbers represent losing and gaining of electrons, respectively.

Conf.	q(adsorbate)	q(Pt)	q(C_1)	q(C_2)	q(C-dimer)
2a	-	-	0.37	0.37	0.74
2b	-	-0.26	0.27	0.27	0.54
3a	0.19	-0.33	0.10	0.30	0.40
3b	-0.45	0.06	0.17	0.17	0.34
3c	0.35	-0.37	0.19	0.19	0.38
4c	-1.05	0.49	0.24	0.24	0.48
5a	-0.47	0.07	0.17	0.17	0.34
5b	-0.69	0.08	0.16	0.16	0.32
6a	-0.12	-0.13	0.15	0.17	0.32
6b	-0.23	-0.03	0.24	0.29	0.53
6c	-0.56	0.10	0.17	0.16	0.33
7a	-0.13	-0.13	0.19	0.33	0.52

7b	0.08	-0.26	0.27	0.28	0.55

[*] q(X) stands for the total charge on the X and the q(C-dimer) represent the total charge of C_1 and C_2 as labeled in Fig. 2.

3.2. The adsorption of reaction species

Based on the most stable structure of the Pt/NG (Fig. 1b), various adsorption sites including the Pt atom, the N atoms and the C atoms are examined to reveal the optimal adsorption configurations of gas molecules. The calculated results indicate that all reactants tend to be adsorbed at the Pt site, and the most stable adsorption configurations with the corresponding geometric parameters and adsorption energies for each of the reactants are depicted in Fig. 3. There was no imaginary frequency observed for each of the stable structures indicating they are local minima in the potential energy surface.

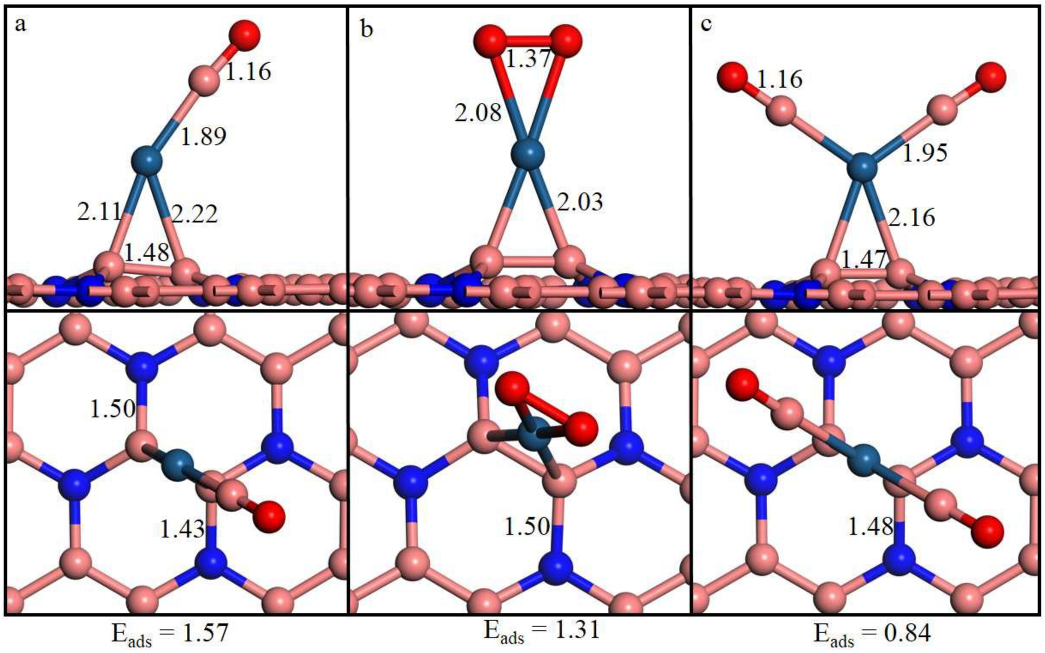

Fig. 3 The optimal adsorption configuration of CO (a), O_2 (b) and 2CO (c) on Pt/NG. The red balls are O atoms.

As shown in Fig. 3a, CO is aslant adsorbed on the Pt/NG forming a Pt-C bond of 1.89 Å. The calculated adsorption energy is 1.57 eV accompanied with about 0.20 electrons transferred from CO to Pt/NG. The single Pt atom gets more electrons as compared with that in the bare Pt/NG, as shown in Table 1. Originating from this charge transfer, the C-O distance is elongated to 1.16 Å from 1.14 Å in a free molecule. Comparing Fig. 3a with Fig. 2b, we find that the structural distortion of the Pt/NG catalyst induced by CO adsorption is insignificant, which confirms that the Pt/NG catalyst is stable for catalyzing CO oxidation.

The adsorbed O_2 molecule prefers to lie parallel to the basal plane of the NG and immediately on the top site of Pt atom, forming two Pt-O bonds of 2.08 Å as shown in Fig. 3b. The adsorption energy of O_2 molecule is 1.31 eV, which is weaker than that of CO. The Mulliken charge analysis indicates that there are about 0.45 electrons transferred from the Pt/NG to the adsorbed O_2 molecule. The completely different charge transfer phenomena between CO and O_2 when they interact with Pt/NG, where CO donates about 0.2 e to the Pt/NG, could be explained by the stronger electronegativity of O_2 than CO. The charge transfer makes the O-O bond elongated to 1.37 Å. Comparing Fig. 3b with Fig. 2b, we find that the Pt-C distances are shortened to 2.03 Å from 2.11 Å due to O_2 adsorption, and the N-C bonds are enlarged to 1.50 Å from 1.45 Å accordingly. This phenomenon is consistent with the strong interaction between Pt and the activated C atoms.

According to the above results, both CO and O_2 tend to be adsorbed at the Pt site instead away from the Pt site. CO will be slightly more preferable to occupy the activated Pt site of Pt/NG when the two reactant gases (CO and O_2) are injected synchronously since the adsorption strength to CO is slightly stronger than that to O_2. Furthermore, the adsorption behavior of the Pt/NG to O_2 or the second CO will be changed when a CO is preadsorbed, which will also influence the subsequent reaction path. Indeed, when a CO is preadsorbed on Pt/NG, the adsorption energy of O_2 is 0.30 eV, whereas the adsorption energy of the second CO is 0.84 eV. Thus, coadsorption of two CO molecules is more preferable than the coadsorption of CO and O_2. The most stable coadsorption structure of two CO molecules on the Pt/NG is shown in Fig. 3c, where a V-shape O-C-Pt-C-O structure is formed with an average adsorption energy of 0.84 eV. The moderate adsorption and small adsorption energy difference between CO and O_2 may facilitate the catalytic reaction of CO oxidation and decrease the reaction barriers accordingly.

The optimized geometric structures of the intermediate product O and the final product CO_2 adsorbed on the Pt/NG are also calculated and will be discussed below.

3.3. The oxidation of CO by O_2

Generally, there are two kinds of reaction mechanisms for CO oxidation, i.e., the Eley-Rideal (E-R) and Langmuir-Hinshelwood (L-H) mechanisms, depending on the adsorption strength of the catalyst to the mixed gases. The L-H mechanism involves the coadsorption of O_2 and CO molecules before reaction, formation of an intermediate state and desorption of the product CO_2 molecule. The E-R mechanism is featured with the reactant CO molecules approaching the already activated O_2. In our study, both mechanisms are investigated comparatively.

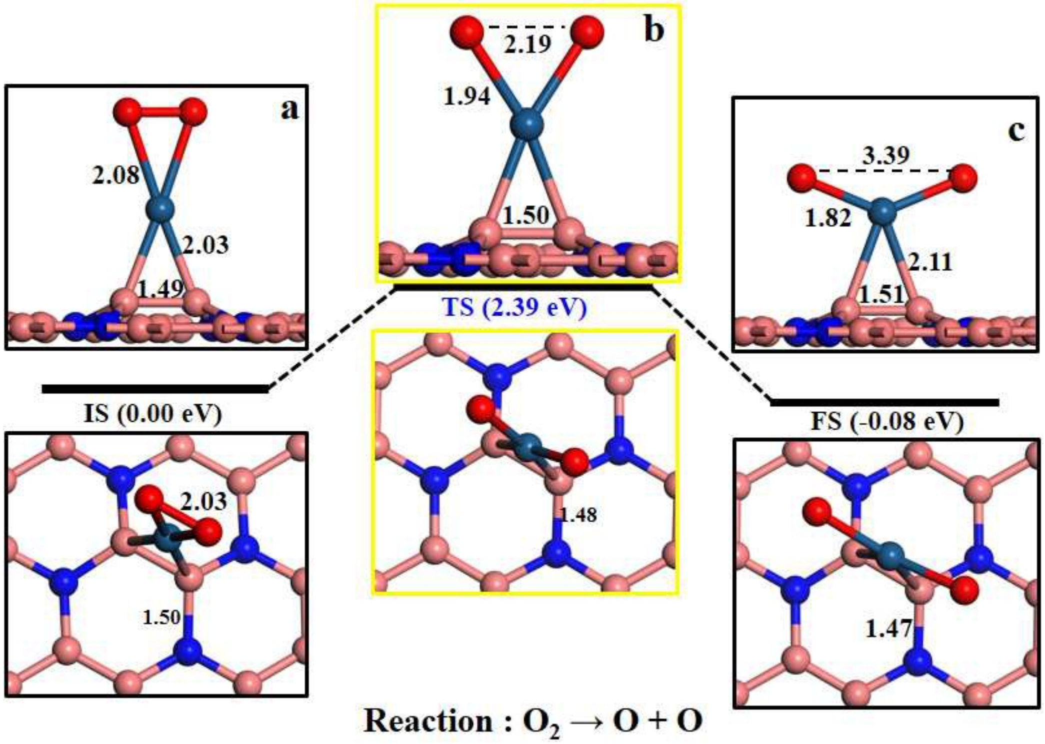

Fig. 4 The dissociation of O_2 on Pt/NG. The transition state is marked by orange pane hereafter.

Since the interaction of CO with Pt/NG is stronger than O_2, the catalytic reaction proceeding by the E-R mechanism may be suppressed. This conjecture could also be testified by the large barrier of O_2 decomposition. To search for the MEP of O_2 decomposition, we selected the most stable adsorption configuration (Fig. 4a) of O_2 as the initial state (IS). The final state (FS) is the structure with two chemisorbed O atoms located symmetrically at the shoulders of Pt (Fig. 4c). The MEP profile and the corresponding geometric configurations are summarized in Fig. 4. From Table 1, we find that the catalyst substrate donates about 0.60 electrons to activate the O_2 molecule. These transferred electrons are primarily from the Pt atom. This result shows that the Pt atom is the active site for O_2 decomposition. The calculated reaction barrier for O_2 dissociation is 2.39 eV with about 0.08 eV energy released. The rather large decomposition barrier of O_2 indicates that the E-R reaction is hard to happen.

In spite of this, the E-R mechanism is also explored in present study in order to compare with the L-H mechanism conveniently. The configuration of a physisorbed CO suspended above the O_2 occupied Pt/NG catalyst is regarded as IS, and the FS is identified with a carbonate-like species (CO_3) located on the Pt atom. The configurations of IS and FS, as well as the corresponding conversion process from IS to FS are depicted in Fig. 5. Firstly, the physisorbed CO progressively approaches the adsorbed O_2, while the O-O and Pt-O bonds elongated simultaneously to respond to the behavior of CO and finally reaches the TS. In TS, the C-O bond in CO expanded to 1.17 Å and the average length of the new formed C-O bonds is 1.81 Å. Passing over the TS, CO completely inserts into the O-O bond forming a carbonate-like FS. The E-R process is exothermic by 3.69 eV, but there is an energy barrier of about 1.81 eV needed be overcome to break the O-O bond and form the new C-O bonds. The results of Mulliken charge analysis indicate that both Pt and NG substrate contribute their electrons to activate the reaction of O_2 with CO (Table 1).

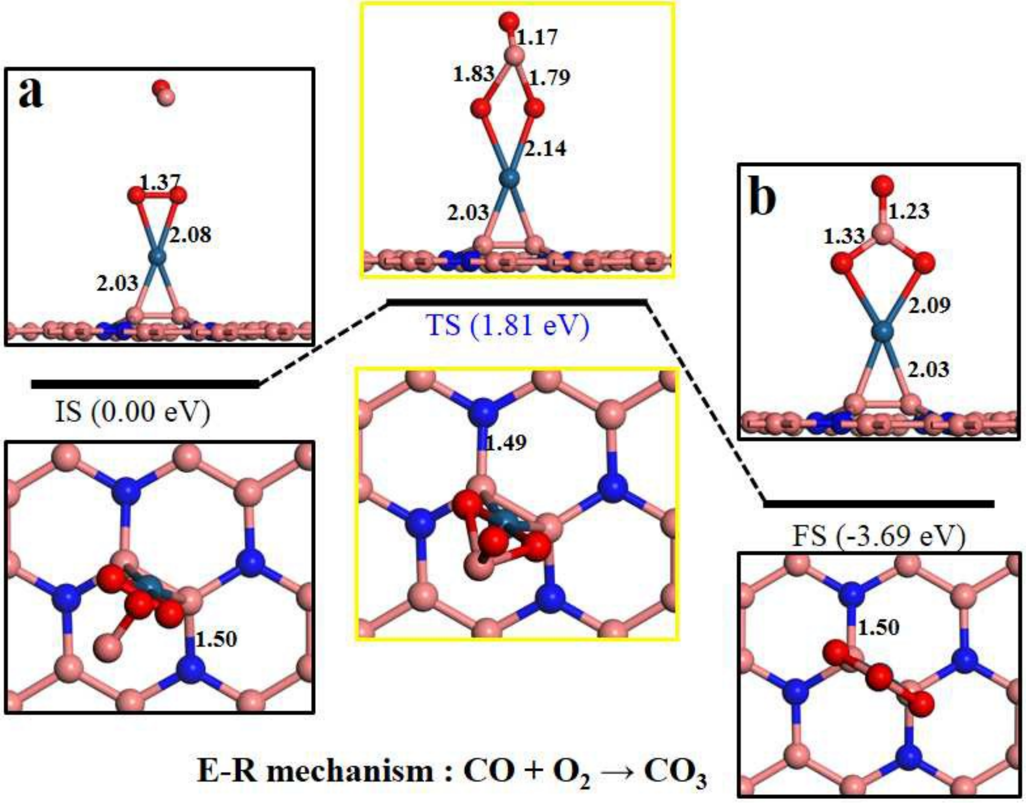

Fig. 5 CO oxidation catalyzed by Pt/NG following the E-R mechanism.

The high barrier implies that the CO oxidation on Pt/NG via the E-R mechanism is almost unpractical. Therefore, we will turn our attention to the L-H mechanism in the following sections. The atomic configurations of various states along the reaction path and the corresponding energy barriers are displayed in Fig. 6. The configuration of CO and O_2 coadsorbed at the Pt atom with Pt-C and Pt-O bonds of 1.91 and 2.14 Å is selected as IS (Fig.

6a). In the IS, the C-O bond and O-O bond are activated to 1.16 and 1.37 Å, respectively. Yet the geometric structure of the Pt/NG system has not too much distortion, which manifested again that the Pt/NG catalyst is stable. The free end of the adsorbed O_2 rotary moves toward the C atom of CO generating a new C-O bond as shown in TS1, which then changes further into a peroxide-like intermediate after rotation and adjustment (Fig. 6b). This conversion process has an energy release of about 0.23 eV and needs to overcome a barrier of 0.59 eV. Subsequently, the formed peroxide-like intermediate can readily decompose with an energy barrier of 0.10 eV. In this dissociation process, the Pt-O-O-C four-membered ring is broken first, forming a CO_2-like molecule and leaving an atomic O adsorbed on the Pt atom (Fig. 6c).

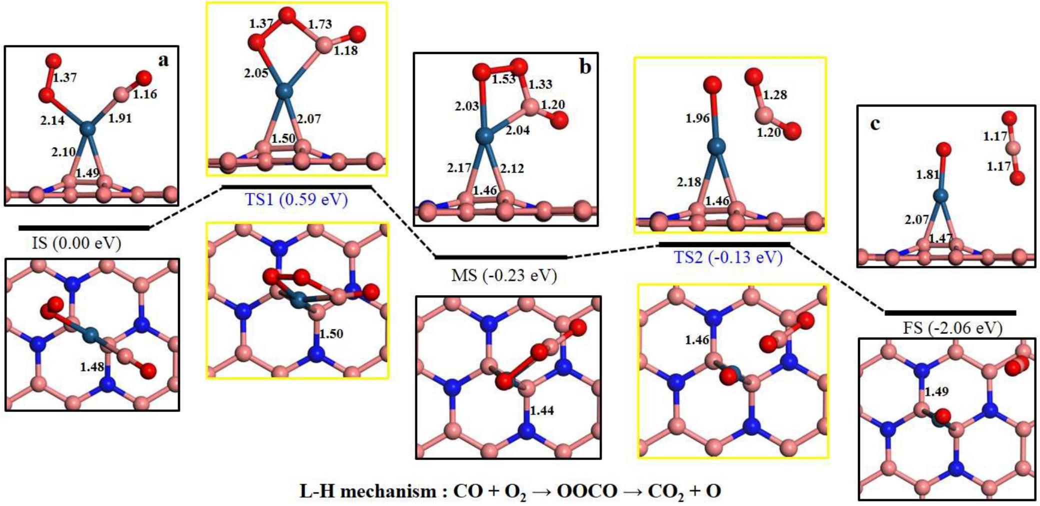

Fig. 6 CO oxidation catalyzed by Pt/NG following the L-H mechanism.

The formed CO_2-like molecule may desorb easily with an atomic O left on the Pt atom, which can be used to oxidize the subsequent coming CO molecule. Once the CO_2 desorbs, the remaining O will be bound directly on the top site of Pt with a Pt-O bond of 1.81 Å. The Pt-C and C-C bonds are shortened to 2.06 and 1.47 Å, respectively, and the N-C bonds are enlarged by about 0.04 Å. The calculated adsorption energy of O is 4.05 eV accompanied with about 0.55 electrons transferred from Pt/NG to the O atom. A configuration of CO staying 3.08 Å away from the adsorbed O is selected as the IS (Fig. 7a) to investigate the reaction of a gaseous CO molecule with the adsorbed O atom over Pt/NG. The product is set as the configuration of a weakly adsorbed CO_2 aslant suspending 2.45 Å above Pt/NG (Fig. 7b) with an adsorption energy of 0.24 eV, which is the most preferable adsorption structure for CO_2. Fig. 7 presents the geometrical structures change and the corresponding energy barrier during the reaction process. In the oxidization process, the C atom of CO approaches the adsorbed O, developing bond with the atomic O and attracting it away from the Pt atom as shown in TS and finally forming a CO_2 as shown in FS. The relative small adsorption energy, large Pt-O distance both indicate that the formed CO_2 could desorb easily from the Pt/NG.

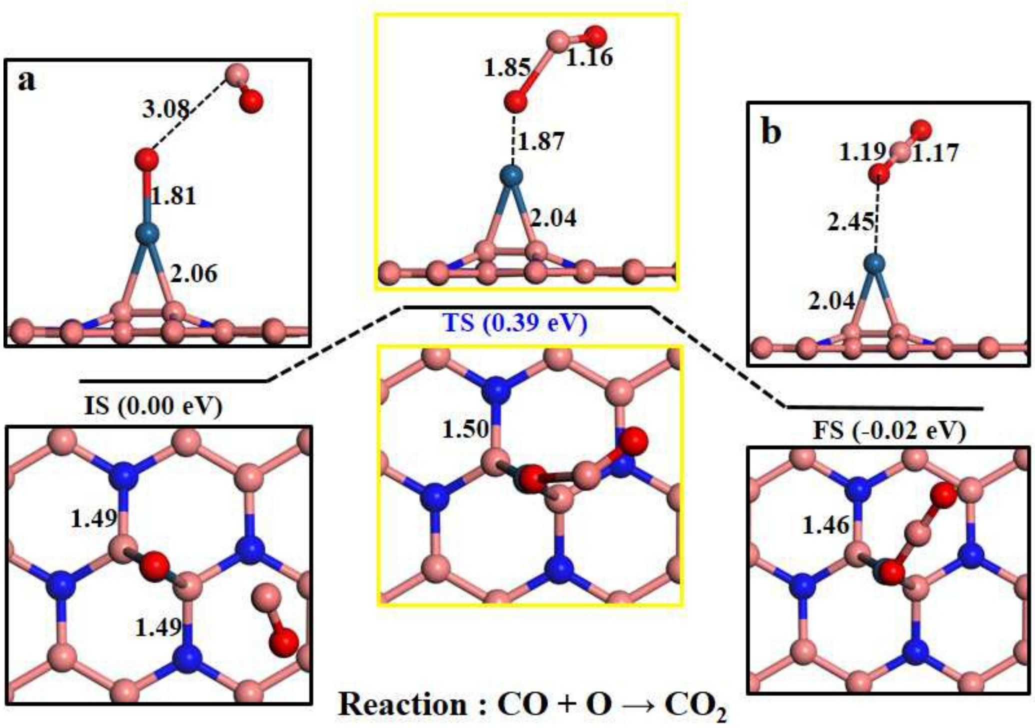

Fig. 7 The minimum energy path for CO oxidation by the dissociative O.

It is noteworthy that the adsorption strength of Pt/NG to CO is stronger than that to O_2 regardless the Pt atom is occupied by the preadsorbed CO or not. Therefore, the active sites of Pt/NG may be covered entirely by CO when it is excess, and the CO oxidation through the normal L-H mechanism may also be unprosperous. The tri-molecular E-R mechanism, which characters with the O_2 being activated by two preadsorbed CO molecules directly, was proposed recently by Mao[7] to solve this problem. The reaction pathway of CO oxidation along the tri-molecular E-R mechanism is displayed in Fig. 8. The O_2 molecule moves evenly toward the coadsorbed CO molecules from the IS (an O_2 suspending above the two coadsorbed CO molecules), bridging the two adsorbed CO molecules and forming an OCO-OCO intermediate product (MS). In this process, two new C-O bonds are formed and the O-O distance is enlarged to 1.48 Å from 1.28 Å in order to match the new C-O bonds. Subsequently, two CO_2-like molecules formed (as shown in TS2) by cleaving the O-O bond, which could desorb easily due to the weak interaction of CO_2 with Pt/NG. The calculated average adsorption energy of CO_2 is 0.24 eV accompanied with about 0.08 electrons transferred to Pt/NG. The reaction barriers (energies) of OCO-OCO formation and dissociation process are 0.06 (0.91) and 0.16 (3.03) eV, respectively, which are both lower than the corresponding values on the Au-embedded boron nitride monolayer catalyst[7]. Apart from this, the Pt/NG is also more efficient for CO oxidation than Pt supported on defective[56], oxidative[14], and metal Ge modified[34] graphene from the energy barrier point of view, and also better than that of Au[7] and Fe[8,57] embedded defective graphene and boron nitride monolayer. The rate-limiting steps and the corresponding reaction energy barriers of CO oxidation on metal-graphene composite catalysts mentioned above are summarized in Table 2 for the convenient of comparison. These results indicate that the Pt/NG catalyst is highly efficient for CO oxidation. Besides, we also find that the adsorbed CO can help to activate O_2 by lowing the activation barriers. The energy barrier for breaking the O-O bond is reduced to 0.16 eV by the preadsorbed CO molecules in the tri-molecular E-R process from the value of 2.39 eV on the bare Pt/NG. The related vibrational frequencies of all the transition states are calculated and all the transition states are identified with only one imaginary frequency. The detailed results are tabulated as Table S1 (supporting information).

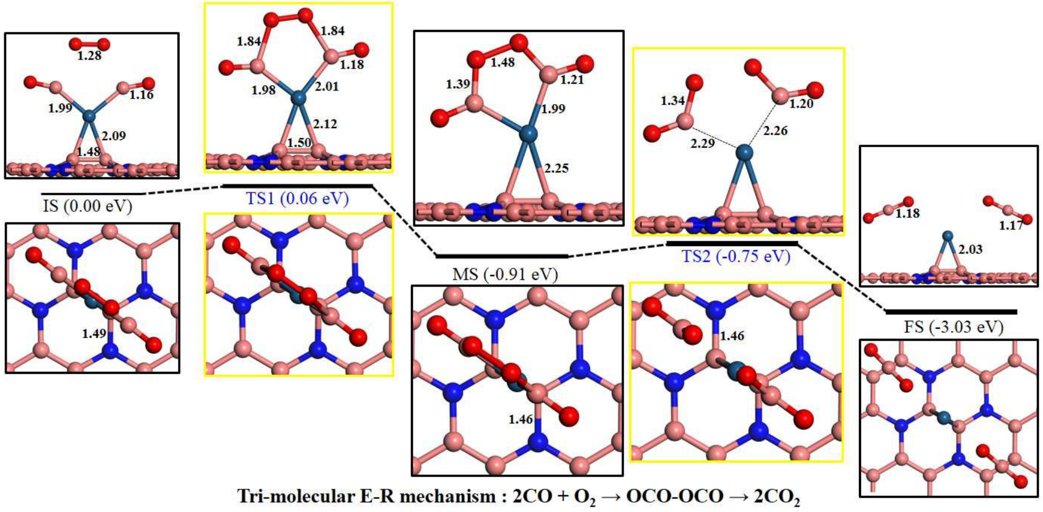

Fig. 8 CO oxidation catalyzed by Pt/NG following the Tri-molecular E-R mechanism.

Table 2. The rate-limiting steps and the corresponding reaction barriers of CO oxidation on various metal-graphene catalysts.

Models	Reaction steps	Barriers	Models	Reaction steps	Barriers
Cu-Gra[6]	CO +O → CO_2	0.54	Fe-Gra[57]	CO +O_2 → CO_3	0.58
Pt-Gra[56]	CO +O → CO_2	0.46	Al-Gra[58]	CO +O_2 → OOCO	0.32
Pt-O/Gra[14]	CO + O_2 → O + CO_2	0.76	Pt-Ge/Gra[34]	CO + O_2 → O + CO_2	0.86
Au-NB[7]	OCO-OCO → $2CO_2$	0.47	Fe-NB[8]	CO +O → CO_2	0.61

The excellent catalytic activity of Pt/NG to CO oxidation could be understood further by the charge analysis. From Table 1, we find that the C_1 and C_2 atoms in the center of the N dopant cluster (Fig. 2a) lose about 0.37 electrons, respectively. The carbon dimer, which loses 0.74 electrons in total, is just the most preferred adsorption site for atomic Pt. Further, the adsorbed Pt atom can be regarded as active site for CO oxidation since it could donate/attract electrons to modulate the adsorption and reaction of CO with O_2. For example, the Pt atom acquires more electrons (0.33 vs 0.26) with CO adsorption than that in the bare Pt/NG system, yet loses electrons (0.06) with O_2 adsorption. Besides, the CO (O_2) loses (gets) more (less) electrons in the coadsorption system than those in the corresponding simplex CO (O_2) adsorption systems. These results indicate that the atomic Pt adsorbed on the NG substrate could tune the electronic properties of different adsorbates and subsequently activate the reaction between CO and O_2. Similar phenomena are observed when O_2 and two CO molecules coadsorbed on the Pt/NG.

4. Conclusions

The excellent stability and catalytic activity of the Pt/NG model catalyst are revealed by the first-principles calculations. The main conclusions are summarized as follows:

(1) The stability of single Pt atom on graphene could be promoted by choosing the appropriate dopant atoms or doping configuration.

(2) The CO oxidation is hard to proceed along normal E-R mechanism for the large barrier of 1.81 eV.

(3) The normal L-H mechanism with an energy barrier of 0.59 eV for OOCO formation is more preferable than the normal E-R mechanism.

(4) The tri-molecular E-R mechanism ($2CO + O_2 \rightarrow OCO\text{-}OCO \rightarrow 2CO_2$) is more preferable than the normal L-H and E-R mechanisms. The intermediate product dissociation step with a barrier of 0.16 eV is the rate-limiting step.

Acknowledgments:

This work is supported by the National Natural Science Foundation of China (Grant No. 11174070, 11474086, 51401078 and U1304518). Parts of the simulations are performed on resources provided by the high-performance computing center of College of Physics and Electronic Engineering in Henan Normal University.

Notes and References:

[a]*College of Physics and Electronic Engineering, Henan Normal University, Xinxiang, 453007, China. E-mail addresses: zslu@henannu.edu.cn (Z. Lu), yzx@henannu.edu.cn (Z Yang)*
[b]*School of Physics, Anyang Normal University, Anyang 455000, China*

[c]*School of Chemistry and Chemical Engineering, Henan Normal University, Xinxiang, 453007, China*

1 M. Ackermann, T. Pedersen, B. Hendriksen, O. Robach, S. Bobaru, I. Popa, C. Quiros, H. Kim, B. Hammer and S. Ferrer, Phys. Rev. Lett., 2005, **25**, 255505.

2 A. Eichler, Surf. Sci., 2002, **3**, 314.

3 I. Nakai, H. Kondoh, T. Shimada, A. Resta, J. N. Andersen and T. Ohta, J. Chem. Phys., 2006, **22**, 224712.

4 M. L. Kimble, A. W. Castleman, R. Mitric, C. Bürgel and V. BonačIc-Koutecký, J. Am. Chem. Soc., 2004, **8**, 2526.

5 C. Zhang, R. Baxter, P. Hu, A. Alavi and M.-H. Lee, J. Chem. Phys., 2001, **11**, 5272.

6 E. Song, Z. Wen and Q. Jiang, J. Phys. Chem. C, 2011, **9**, 3678.

7 K. Mao, L. Li, W. Zhang, Y. Pei, X. C. Zeng, X. Wu and J. Yang, Sci. Rep., 2014, **4**, 5441.

8 P. Zhao, Y. Su, Y. Zhang, S.-J. Li and G. Chen, Chem. Phys. Lett., 2011, **1**, 159.

9 Q. Sun, Z. Li, A. Du, J. Chen, Z. Zhu and S. C. Smith, Fuel, 2012, **96**, 291.

10 J. Lin, A. Wang, B. Qiao, X. Liu, X. Yang, X. Wang, J. Liang, J. Li, J. Liu and T. Zhang, J. Am. Chem. Soc., 2013, **41**, 15314.

11 Y. Tang, Z. Yang and X. Dai, Phys. Chem. Chem. Phys., 2012, **48**, 16566.

12 Y. Tang, Z. Yang, X. Dai, D. Ma and Z. Fu, J. Phys. Chem. C, 2013, **10**, 5258.

13 Y. Tang, X. Dai, Z. Yang, Z. Liu, L. Pan, D. Ma and Z. Lu, Carbon, 2014, **71**,139.

14 Y. Tang, X. Dai, Z. Yang, L. Pan, W. Chen, D. Ma and Z. Lu, Phys. Chem. Chem. Phys., 2014, **17**, 7887.

15 B. Qiao, A. Wang, X. Yang, L. F. Allard, Z. Jiang, Y. Cui, J. Liu, J. Li and T. Zhang, Nature Chem., 2011, **8**, 634.

16 Y. Tang, Z. Yang and X. Dai, J. Chem. Phys., 2011, **22**, 224704.

17 B. Huang, Z. Li, Z. Liu, G. Zhou, S. Hao, J. Wu, B.-L. Gu and W. Duan, J. Phys. Chem. C, 2008, **35**, 13442.

18 Z.-H. Sheng, L. Shao, J.-J. Chen, W.-J. Bao, F.-B. Wang and X.-H. Xia, Acs Nano, 2011, **6**, 4350.

19 C. Zhang, L. Fu, N. Liu, M. Liu, Y. Wang and Z. Liu, Adv. Mater., 2011, **8**, 1020.

20 D. Deng, X. Pan, L. Yu, Y. Cui, Y. Jiang, J. Qi, W.-X. Li, Q. Fu, X. Ma and Q. Xue, Chem. Mater., 2011, **5**, 1188.

21 C. Zhang, N. Mahmood, H. Yin, F. Liu and Y. Hou, Adv. Mater., 2013, **35**, 4932.

22 M. Latorre‐Sánchez, A. Primo and H. García, Angew. Chem. Int. Edit., 2013, **45**, 11813.

23 J. Wu, Z. Yang, X. Li, Q. Sun, C. Jin, P. Strasser and R. Yang, J. Mater. Chem. A, 2013, **34**, 9889.

24 L. Qu, Y. Liu, J.-B. Baek and L. Dai, ACS nano, 2010, **3**, 1321.

25 L. Zhang and Z. Xia, J. Phys. Chem. C, 2011, **22**, 11170.

26 X. Zhang, Z. Lu, Z. Fu, Y. Tang, D. Ma and Z. Yang, J. Power Sources, 2014, **276**, 222.

27 X. Zhang, Z. Lu, Y. Tang, Z. Fu, D. Ma and Z. Yang, Phys. Chem. Chem. Phys., 2014, **38**, 20561.

28 X. Zhang, Z. Lu, Y. Tang, D. Ma and Z. Yang, Catal. Lett., 2014, **6**, 1016.

29 Y. Wang, Y. Shao, D. W. Matson, J. Li and Y. Lin, ACS nano, 2010, **4**, 1790.

30 B. Xiong, Y. Zhou, Y. Zhao, J. Wang, X. Chen, R. O'hayre and Z. Shao, Carbon, 2013, **52**, 181.

31 F. Su, Z. Tian, C. K. Poh, Z. Wang, S. H. Lim, Z. Liu and J. Lin, Chem. Mater., 2009, **3**, 832.

32 M. N. Groves, C. Malardier-Jugroot and M. Jugroot, J. Phys. Chem. C, 2012, **19**, 10548.

33 X. Liu, Y. Sui, T. Duan, C. Meng and Y. Han, Catal. Sci. Technol., 2015, **5**, 1658.

34 Y. Tang, Z. Yang, X. Dai, Z. Lu, Y. Zhang and Z. Fu, J. Nanosci. Nanotechno., 2014, **9**, 7117.

35 B. Delley, J. Chem. Phys., 1990, **1**, 508.

36 S. Grimme, J. Comput. Chem., 2006, **15**, 1787.

37 J. P. Perdew, K. Burke and M. Ernzerhof, Phys. Rev. Lett., 1996, **18**, 3865.

38 T. A. Halgren and W. N. Lipscomb, Chem. Phys. Lett., 1977, **2**, 225.

39 T. Xing, Y. Zheng, L. H. Li, B. C. Cowie, D. Gunzelmann, S. Z. Qiao, S. Huang and Y. Chen, ACS nano, 2014, **7**, 6856.

40 D.-W. Kim, O. L. Li and N. Saito, Phys. Chem. Chem. Phys., 2014, **28**, 14905.

41 D. H. Lee, W. J. Lee, W. J. Lee, S. O. Kim and Y.-H. Kim, Phys. Rev. Lett., 2011, **17**, 175502.

42 L. Lin, Q. Zhu and A.-W. Xu, J. Am. Chem. Soc., 2014, **31**, 11027.

43 S. Kattel and G. Wang, J. Mater. Chem. A, 2013, **36**, 10790.

44 U. I. Koslowski, I. Abs-Wurmbach, S. Fiechter and P. Bogdanoff, J. Phys. Chem. C, 2008, **39**, 15356.

45 Z. Lu, G. Xu, C. He, T. Wang, L. Yang, Z. Yang and D. Ma, Carbon, 2015, **84**,500.

46 S. Kattel, P. Atanassov and B. Kiefer, Phys. Chem. Chem. Phys., 2013, **1**, 148.

47 S. Chao, Z. Lu, Z. Bai, Q. Cui, J. Qiao, Z. Yang and L. Yang, Int. J. Electrochem. Sci, 2013, **8**, 8786.

48 Y. Feng, F. Li, Z. Hu, X. Luo, L. Zhang, X.-F. Zhou, H.-T. Wang, J.-J. Xu and E. Wang, Phys. Rev. B, 2012, **15**, 155454.

49 C. Fonseca Guerra, J. W. Handgraaf, E. J. Baerends and F. M. Bickelhaupt, J. Comput. Chem., 2004, **2**, 189.

50 W. Song, C. Popa, A. P. Jansen and E. J. Hensen, J. Phys. Chem. C, 2012, **43**, 22904.

51 J. Lin, B. Qiao, J. Liu, Y. Huang, A. Wang, L. Li, W. Zhang, L. F. Allard, X. Wang and T. Zhang, Angew. Chem. Int. Edit., 2012, **12**, 2920.

52 M. Moses-Debusk, M. Yoon, L. F. Allard, D. R. Mullins, Z. Wu, X. Yang, G. Veith, G. M. Stocks and C. K. Narula, J. Am. Chem. Soc., 2013, **34**, 12634.

53 A. A. Herzing, C. J. Kiely, A. F. Carley, P. Landon and G. J. Hutchings, Science, 2008, **5894**, 1331.

54 W.-C. Ding, X.-K. Gu, H.-Y. Su and W.-X. Li, J. Phys. Chem. C, 2014, **23**, 12216.

55 P. Hu, Z. Huang, Z. Amghouz, M. Makkee, F. Xu, F. Kapteijn, A. Dikhtiarenko, Y. Chen, X. Gu and X. Tang, Angewandte Chemie, 2014, **13**, 3486.

56 X. Liu, Y.Sui, T. Duan, C. Meng and Y. Han, Phys. Chem. Chem. Phys., 2014, **16**, 23584.

57 Y. Li, Z. Zhou, G. Yu, W. Chen and Z. Chen, J. Phys. Chem. C, 2010, **114**, 6250.

58 Q. Jiang, Z. Ao, S. Li and Z. Wen, RSC Adv., 2014, **4**, 20290.